Ultrasonics Sonochemistry 77 (2021) 105669

Contents lists available at ScienceDirect

Ultrasonics Sonochemistry

journal homepage: www.elsevier.com/locate/ultson

Investigation into cavitational intensity and COD reduction performance of the pinned disc reactor with various rotor-stator arrangements

Jurij Gostiša [a], Mojca Zupanc [a], Matevž Dular [a], Brane Širok [a], Marjetka Levstek [b], Benjamin Bizjan [a,*]

[a] Faculty of Mechanical Engineering, University of Ljubljana, Ljubljana, Slovenia
[b] JP CCN Domzale-Kamnik d.o.o., Domzale-Kamnik WWTP, Domzale, Slovenia

ARTICLE INFO

Keywords:
Hydrodynamic cavitation
Wastewater treatment
Pinned disc reactor
Flow visualization
Performance evaluation

ABSTRACT

In this study, the hydrodynamic cavitation and wastewater treatment performance of a rotary generator with pin disk for hydrodynamic cavitation are investigated. Various geometrical features and arrangements of rotor and stator pins were evaluated to improve the configuration of the cavitation device. The pilot device used to perform the experiments was upgraded with a transparent cover that allows visualization of the hydrodynamic cavitation in the rotor-stator region with high-speed camera and simultaneous measurement of pressure fluctuations. Based on the hydrodynamic characteristics, three arrangements were selected and evaluated with respect to the chemical effects of cavitation on a 200-liter wastewater influent sample. The experimental results show that the rotational speed and the spacing of the rotor pins have the most significant effect on the cavitation intensity and effectiveness, while the pin diameter and the surface roughness are less significant design parameters. Cavitation intensity increases with pin velocity, but can be inhibited if the pins are arranged too close together. At best configuration, COD was reduced by 31% in 15 liquid passes, consuming 8.2 kWh/kg COD. The number of liquid passes also proved to be an important process parameter for improving the energy efficiency.

1. Introduction

As the global population is becoming increasingly urbanized, the already scarce water sources are threatened by growing surface and groundwater pollution. Wastewater (WW) discharged from industry and households contains a multitude of potentially hazardous contaminants such as industrial chemicals, personal care products and pharmaceuticals, bacteria, viruses and microplastics. The ever-growing list of microcontaminants presents a major challenge to the operation of conventional wastewater treatment plants (WWTP) as some contaminants may significantly increase the WW treatment cost and duration, or even interfere with the treatment processes, thus rendering them inadequate. Increasingly stringent environmental legislation in developed countries has led to research of more efficient WW treatment technologies with lower environmental footprint (i.e., no addition of external chemicals and low energy consumption) that can be considered as green technologies.

One of such promising technologies where no external additives are needed is hydrodynamic cavitation (HC) that encompasses formation, growth, and collapse of vapor bubbles in a liquid due to mechanically induced local pressure drop and recovery. Rapid vapor bubble collapse is associated with extreme local pressure, velocity and temperature [1,2] resulting in mechanical disintegration and chemical degradation of pollutants. While mechanical effects such as shockwaves and shear forces typically lead to disintegration of particles [3,4] chemical effects manifest as formation of hydroxyl radicals ($^{\bullet}$OH) and other reactive species, that drive oxidative destruction of organic pollutants [5]. Compared to other cavitation types (e.g. acoustic cavitation), HC has the advantage of lower treatment cost and better scalability when employed for wastewater treatment (WWT) [1]. Several different cavitator designs have been successfully employed for advanced oxidation of dissolved organic compounds (a review provided in [1,6,7]) and disinfection (a review provided in [2,8]) of WW. These include orifice plates [9,10], venturi tubes [10,11], vortex cavitation [12], and rotating devices

Abbreviations: AOP, advanced oxidation process; COD, total chemical oxygen demand; COD_i, initial COD; EC, electric conductivity of wastewater; DO, dissolved oxygen; HC, hydrodynamic cavitation; PD, pinned disc; RGHC, rotating generator of hydrodynamic cavitation; SD, serrated disc; WW, wastewater; WWT, wastewater treatment; WWTP, wastewater treatment plant.

* Corresponding author.
E-mail address: benjamin.bizjan@fs.uni.lj.si (B. Bizjan).

https://doi.org/10.1016/j.ultsonch.2021.105669
Received 17 May 2021; Received in revised form 9 July 2021; Accepted 11 July 2021
Available online 16 July 2021

[13–24] that will be hereinafter referred to as rotational generators of hydrodynamic cavitation (RGHC).

Main advantages of rotational cavitation generators (namely, rotor–stator-interaction and similar RGHC designs) over simpler venturi and orifice designs include lower specific energy consumption, better scalability and no requirement for a separate high-pressure pump while achieving similar cavitation intensity [2,6]. This, on the other hand, comes at the expense of a greater complexity of internal geometry and cavitation mechanism as opposed to fixed-geometry cavitators. Several different RGHC designs have been developed in the recent years, including dimpled rotors [14,15,18,19,21,23] vaned rotor–stator devices [20], serrated discs [16,17,25,26,27], and pinned discs [22]. Dimpled rotors have been proven effective in sludge solubilization [3,15], destruction of cyanobacteria [18] and in esterification of vegetable oil [23] but are limited by relatively low liquid throughputs and somewhat modest COD removal performance. The vaned rotor–stator reactor presented by Cerecedo and co-workers [20] was very effective in destruction of both gram-negative and gram-positive bacteria, albeit with a limitation that the device only operated on small batches of liquid rather than continuously.

Unlike the RGHC designs discussed above, serrated disc (SD) and pinned disc (PD) variants of rotary cavitating devices are easily scalable, allowing for high wastewater and sludge processing capacity [17,22]. The performance of SD RGHC has so far been studied on both lab-scale [25,26,28,29] and pilot-scale [16,17,27,30] with promising results regarding sludge solubilization, fibrillation of conifer fibers, wastewater disinfection and degradation of various dissolved organic compounds (i.e. pharmaceuticals, bisphenols). However, the most commonly used SD RGHC design with radial serrations requires a low and uniform rotor–-stator clearance for optimal operation [27] and is thus prone to clogging or damage by larger solid particles. To overcome these limitations, Gostiša and co-workers [22] proposed a more robust, novel pinned disc design and evaluated its performance against a SD RGHC of the same rotor size. Results of the study suggest that at the same rotational speed and liquid flow rate, the pinned disc generates more intense cavitation than the serrated disc, while also consuming significantly less energy per liquid pass and per mass of COD removed [22]. For these reasons, the PD RGHC is so far the most favourable of existing RGHC designs regarding COD removal from municipal WW and should be furthermore investigated as a green oxidation process device.

In comparison with SD and other RGHC designs, the PD RGHC prototype studied by Gostiša and co-workers [22] represents a significant improvement in COD removal efficiency and specific energy consumption. However, the energy consumption is still by 1–2 orders of magnitude larger than in the case of conventional biological treatment. Consequently, potential PD RGHC applications are still limited to WW pretreatment and removal of toxic chemicals that could threaten the following biological treatment. To improve the feasibility of the PD RGHC for large scale WWT, its design must be optimized to reduce the environmental footprint through improved energy efficiency. To attain this goal, the present paper aims to investigate the hydrodynamic performance of various PD RGHC operational and design parameters, particularly the pinned disc geometry as well as their chemical efficiency (i.e. COD reduction) on municipal WWTP influent. WW influent is mostly composed of proteins, carbohydrates and lipids, oxidation of which by OH radicals was reported by Zupanc and co-workers [8].

The main objectives of this study were thus to:

)1) analyze the hydrodynamic cavitation characteristics for various combinations of rotor and stator geometry on both integral and local level,
)2) determine the RGHC geometry and operating conditions for effective COD removal from influent WW samples (in terms of COD reduction and specific energy consumption).

2. Materials and methods

2.1. Rotating generator of hydrodynamic cavitation

A pilot scale RGHC with pinned disc rotor and stator discs was primarily designed and evaluated with respect to WWT potential by Gostiša and co-workers [22] as a more robust and energy efficient alternative to serrated disc and other RGHC designs. Rotor and stator discs of the RGHC in the present study were equipped with replaceable cylindrical pins equidistantly distributed on the disc circumference to induce cavitation in the wake region behind the pins (Fig. 1). Small gap between of high velocity passing rotor and stator pins was implemented to induce pressure fluctuations and therefore allow for a higher intensity of cavitation cloud collapses. Up to 16 rotor pins (diameter D_R) and 15 stator pins (diameter D_S) were arranged on the dividing circles with 174 mm and 145 mm diameters, as depicted in the Fig. 1.

Studies previously performed on a single cylinder [31,32] showed different cavitation regimes to be attainable by varying the fluid velocity and inlet pressure. Therefore, various pin layouts were defined by varying number of pins, pin diameter and surface treatment. Rotor can take up to 16 pins, while 15 stator pins with 12 mm diameter were used in all configurations. Rough surface of the pins (Fig. 1) was attained by the knurling manufacturing process where a diamond shaped pattern was rolled into the pin at 30° spiral angle with 1 mm pitch and 90° profile angle.

2.2. Hydrodynamic cavitation experimental setup

Hydrodynamic performance of the RGHC was evaluated on the experimental setup depicted in Fig. 2. The RGHC (Fig. 2 – 1) is driven by variable frequency drive controlled asynchronous motor (Fig. 2 – 2). The RGHC is installed in a closed-circuit pipeline with throttling valves at the pressure on the suction side (Fig. 2 – 3, 5), and a 1000 L reservoir (Fig. 2 – 4) for the storage of the treated liquid. Static pressure was measured by ABB 2600 T absolute pressure transducer (Fig. 2 - a) and pressure head by ABB 2600 T differential pressure transducer (Fig. 2 – b) with measurement accuracy of both being ± 0.04 %. Flow rate was measured by electromagnetic flow meter ABB WaterMaster DN40 (Fig. 2 – c) with measurement accuracy ± 0.4 %. Cavitation regimes were evaluated optically by visualization with Photron Mini UX100 high-speed camera (Fig. 2 – e) with 10 kHz acquisition rate and image resolution of 1280 × 480 pixels. The stainless-steel stator disc and housing cover of the RGHC were replaced with transparent plexiglass substitutes to provide unobstructed view of the cavitating flow in the rotor–stator interaction zone. While a direct view of the observed area was obstructed by the inlet pipe flange, a mirror positioned at a 45° angle was used (Fig. 2 – bottom left) and the visualization area was illuminated with a diffuse LED light source. Furthermore, visualization was coupled with simultaneous pressure measurement with Teledyne Reason hydrophone, type TC4013 (Fig. 2 – d) with 100 kHz sampling frequency. The inlet pressure p_s was not measured directly but was calculated as $p_s = p_p - \Delta p$.

The mechanical and chemical efficiency of the PD RGHC was investigated at an urban WWTP designed for 149,000 population equivalent and treating approx. 20000 m3 of WW per day. To be able to compare the effectiveness of the selected PD RGHC arrangements, the initial WW sample used was the same for all performed experiments (E1–E3). Thus 1000 L of WW influent was taken directly after the primary treatment and before the biological treatment and was stored in a separate container. To assure representative sampling, the initial sample was continuously mixed using a propeller agitator. Prior each experiment, a 200 L sample was pumped from the container into the RGHC reservoir, and the experiments were conducted on the same day in the time span of 4 h.

Based on the evaluation of hydrodynamic and cavitation characteristics (see Section 3.1) performed on drinking water samples, three different operating regimes and corresponding RGHC layouts were

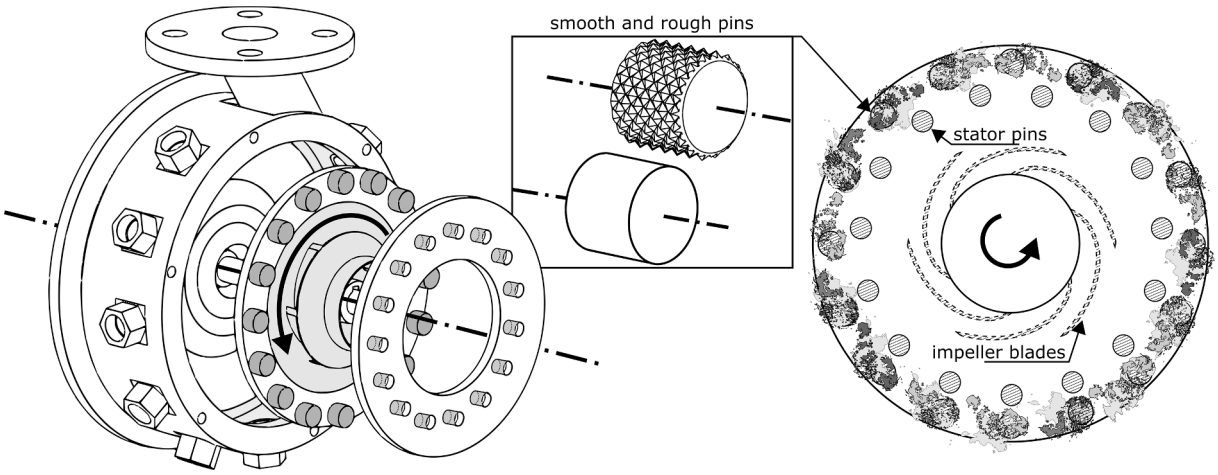

Fig. 1. Pinned disc RGHC design with either smooth or rough stator and rotor pins (left) and cavitation vortices in the Karman street behind the cylinders (right).

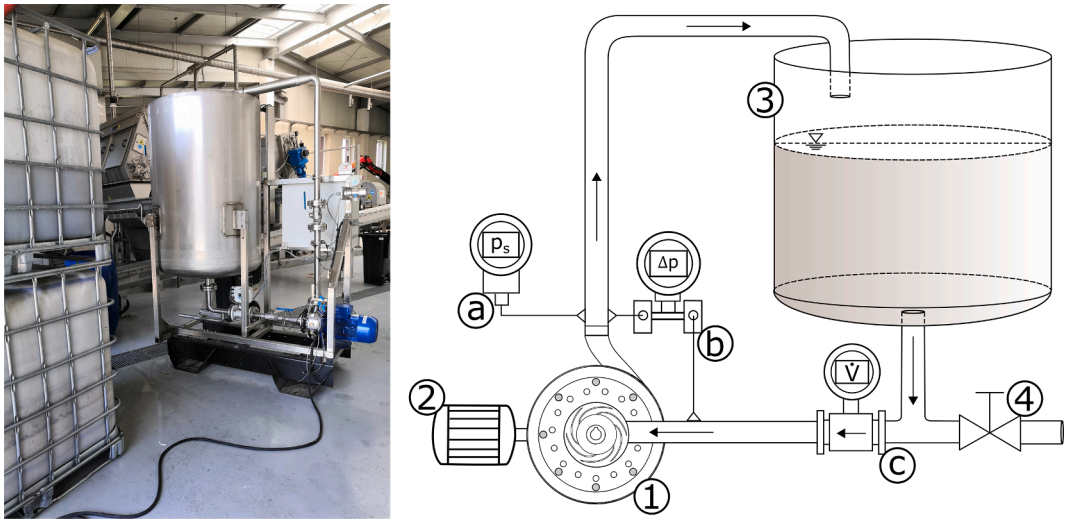

Fig. 2. Key elements of the test rig: 1 – RGHC, 2 – 3-phase asynchronous motor, controlled by variable frequency drive, 3 – pressure side throttling valve, 4 – 1000 L tank, 5 – suction side throttling valve, 6 – discharge valve. Measurement equipment: a – absolute pressure transducer, b – differential pressure transducer, c – electromagnetic flow meter, d – hydrophone, e – high-speed camera.

chosen (Table 1). Due to the strong effect of RGHC's rotational speed on cavitation intensity, all conditions were selected close to the motor's rated rotational speed (2700–3000 RPM) and power (5.2–6.5 kW). The three treatments were compared based on the same amount of cavitation passes, $N_p = \frac{Q \cdot t}{V}$, where Q is the volume flow rate of water, t is the time passed since the start of cavitation process and V is the volume of treated water in the tank.

0.5 L of sample was taken at the beginning of the experiment and after 15 N_p for the analysis of COD. Prior to the COD analysis, the samples were homogenized by mixing.

3. Wastewater sample preparation and analysis

The efficiency of the PD RGHC was assessed by measuring COD, pH, dissolved oxygen (DO), conductivity (EC) and temperature, before and after cavitation. COD of non-filtered samples was determined using Hach-Lange cuvette LCK 514 test and DR/3900 spectrophotometer (Hach-Lange, Germany). Analysis of COD was done in duplicates that never differed by more than ± 2.3 % of the reported average values. pH, DO and conductivity were measured using a Hach-Lange multimeter HQ430d and Intellical PHC725, LD0101 and CDC401 probe, respectively (Hach-Lange, Germany). Temperature was measured using a Flir 566 IR thermometer with measurement range from −60 to 650 °C and accuracy ± 1 °C.

Table 1
Experimental conditions for the three sets of experiments on WW samples.

Experiment	Stator pin layout	Rotor pin layout	n (RPM)	V, N_p	Δp (kPa)	Q (L/s)	P (kW)
E1	Φ12 mm × 15, smooth	Φ16 mm × 8, rough	2700	200 L, sampling at 15 passes	65	8.5	5.3
E2		Φ10 mm × 8, smooth	3000		65	7.7	5.2
E3		Φ10 mm × 16, smooth	3000		93	8.5	6.5

4. Results and discussion

4.1. Evaluation of hydrodynamic and cavitation characteristics

The performance and efficiency of investigated pinned rotor designs can be studied on both integral and local levels, using pressure measurement and high-speed imaging data. The high-speed imaging method has already been employed to investigate cavitation phenomena in the wake stationary cylinders [31] as well as moving pins [22]. Flow structure images in the rotor–stator interaction zone (Fig. 3) are useful for characterization of cavitation structures appearing at different pin arrangements and operating conditions of the RGHC. Hydrodynamic cavitation is manifested as vapor clouds attached to the downstream section of rotating pins (Fig. 3) that intermittently collapse and reappear. Vapor cloud size can be observed to increase when pin diameter is increased (Fig. 3a, b), or when rotational speed of the rotor is increased (Fig. 3b, c).

A highly efficient RGHC is expected to produce intense cavitation with frequent and abrupt vapour cloud collapses at large volume flow rates of treated WW and low specific energy consumption (i.e. energy consumed per unit of processed liquid volume). To improve the RGHC configuration with respect to the current state-of-the-art, three different geometric parameters were investigated, namely the diameter, circumferential spacing and surface roughness of rotor pins. Hydrodynamic operating points (i.e. liquid flow rate and differential pressure across RGHC) to facilitate the evaluation of RGHC performance were selected based on findings of our previous study [22]. The latter showed that neither suction nor pressure side throttling were having any positive effects on COD removal. Therefore, the current study is primarily focused on operation with highest possible rotational velocity in combination with given pin configuration so that the maximum possible extent of cavitation can be achieved for available power rating of the electric motor.

The hydrodynamic performance of multiple RGHC configurations was evaluated based on the hydrodynamic characteristics, namely pressure head Δp and power consumption P. These are given as a function of the flow rate Q, obtained by flow rate regulation with the pressure side valve and shown in the Figs. 4a–4c. The suction side throttling valve was kept fully open in all experiments following recommendations from our previous study [22].

Several observations can be made regarding diagrams presented in Figs. 4a–4c. Firstly, pins contribute a substantial fraction of the total pressure head - in some cases more than 50 %, meaning that Δp generated by rotating protrusions exceeds Δp generated by the pump impeller. Evidently, the contribution to Δp is in correlation to the number of pins arranged about the rotor (in other words, pin circumferential spacing) as more densely arranged pins produce greater Δp at a given Q, while also consuming more power. In the case of pins with 16 mm diameter, the power rating of the motor poses the limitation to operation with just 8 pins. Pressure head curves are also affected by pin diameter and surface roughness, albeit to a lesser degree. Δp can be seen to slightly increase as smooth pins are replaced by rough-surface ones, but so does the power consumed by the RGHC at the given flow rate. The same observation applies when pin diameter is increased since higher diameter pins possess a larger cross section area, resulting in larger drag force exerted on the pins and resultant force accelerating the liquid.

Besides the integral level analysis of RGHC operation ($\Delta p(Q)$ diagrams, Figs. 4a–4c), time series of hydrophone-measured pressure p and cavitation cloud area A (obtained from high-speed camera recordings) were also acquired and analyzed. The acquisition of hydrophone pressure time series $p(t)$ was straightforward as hydrophone pressure fluctuations were linearly proportional to measured hydrophone voltage (35.5 kPa/V). On the other hand, calculation of $A(t)$ required image processing prior to time series acquisition. To ensure a correct segmentation of vapor and liquid phase, high-speed images were processed following an algorithm shown in Fig. 5. First, raw images (Fig. 5a) were temporally averaged to obtain the mean background image (Fig. 5b). Then, the mean image was subtracted from instantaneous images to obtain difference images (Fig. 5c). As a result of image subtraction, background areas with negligible vapor concentration were largely removed, while the vapor cloud region was also corrected for the effect of uneven background illumination. In the next step, a binary mask was created by gray level thresholding (Fig. 5d) followed by morphological closing to remove small black and white areas (Fig. 5e). Time series $A(t)$ was obtained as the area of mask (white region in Fig. 5e). Lastly, Fig. 5f represents the intersection of the difference image with the mask image to verify that the gray level threshold was selected correctly to include the complete cavitation cloud while excluding reflections and other artefacts. Although cavitation structures can be observed on the pin leading edge and in the 1 mm axial gap between pins and the plexiglass cover, only the dynamics of the vapour cloud in the pin downstream region was included in subsequent analysis.

Following the image processing algorithm presented in Fig. 5, cavitating flow regimes can now be visually and quantitatively analyzed. In Fig. 6, the temporal development of cavitating structures is compared for four operating conditions (also consider Table 2) selected by variation of RGHC operating parameters (namely, the pin number, spacing

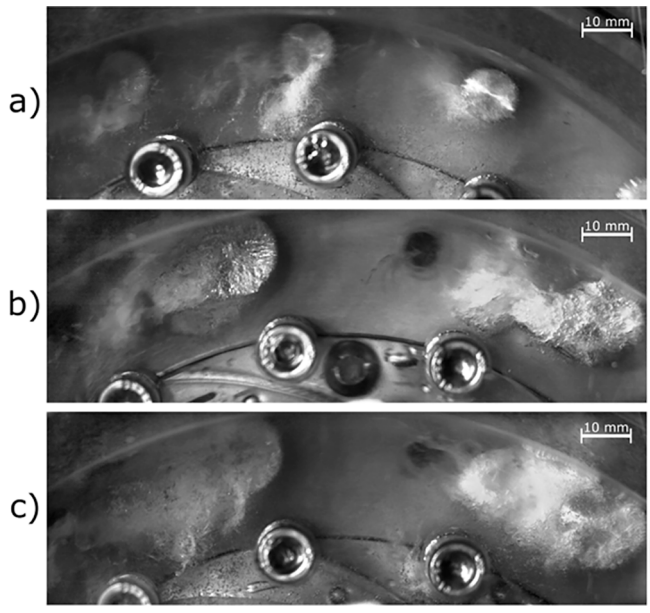

Fig. 3. Flow structures in the rotor–stator interaction region of the RGHC (disc rotation is clockwise): a) $D_R = 10$ mm (16 rough surface pins), $n = 2700$ RPM, $Q = 8.1$ L/s, $\Delta p = 128$ kPa; b) $D_R = 16$ mm (8 smooth surface pins), $n = 2700$ RPM, $Q = 9.5$ L/s, $\Delta p = 79.5$ kPa; c) $D_R = 16$ mm (8 smooth surface pins), $n = 3000$ RPM, $Q = 9.9$ L/s, $\Delta p = 121$ kPa.

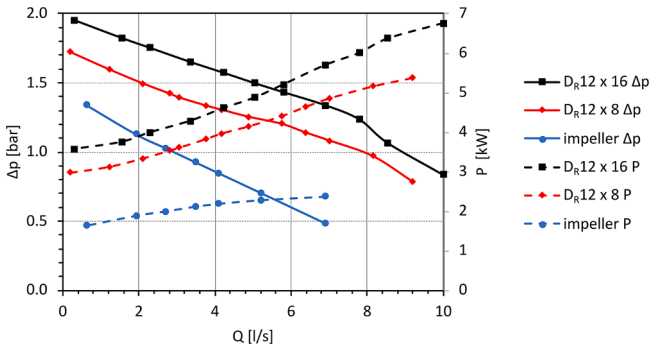

Fig. 4a. Hydrodynamic characteristics for various RGHC configurations - effect of the pin number (circumferential spacing).

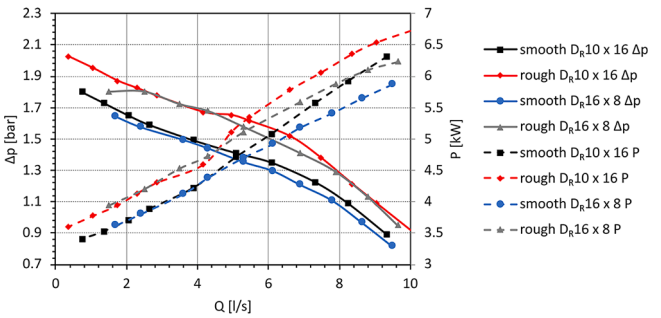

Fig. 4b. Hydrodynamic characteristics for various RGHC configurations – effect of the pin diameter for different number of pins.

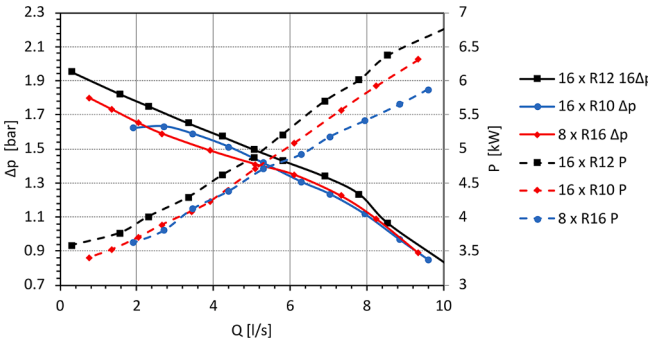

Fig. 4c. Hydrodynamic characteristics for various RGHC configurations – effect of the pin surface roughness.

and surface roughness, as well as rotor speed). $t = 0$ ms corresponds to the reference starting rotor pin position in each recorded imaging sequence. Due to differences in image sequence length, flow structure comparison in Fig. 6 is constrained to the interval 1 ms $\leq t \leq$ 3 ms. As seen in Fig. 6, a large portion of cavitation structures is permanently attached to the pin surface, with smaller clouds detaching from the main cloud and collapsing shortly thereafter. Measurements with 16 mm rotor pins generated visibly larger cavitation structures than the measurement with 10 mm rotor pins, which is an expected result since pins with a smaller cross section generate a smaller low-pressure zone downstream of the pin. Also, imaging data presented in Fig. 6 suggests that for a pin of given diameter, the cavitation intensity and cavitation cloud area is increased when rotational speed of the rotor is increased from 2700 RPM to 3000 RPM, as this causes the cavitation number, $\sigma = 2(p_s\text{-}p_v)/\rho v^2$, to drop ($v$ is pin circumferential velocity). Pin surface roughness can also be observed to affect the cavitating flow dynamics, although less significantly than pin diameter and circumferential velocity.

Regions of interest shown in Fig. 6 were used for acquisition of time series of hydrophone pressure, $p(t)$, and cavitation cloud area, $A(t)$. Unlike p that was measured as a continuous time series, a separate time series of A_i was obtained for each (i-th) rotor pin passage through the camera recording area, on a total of 80 pin passages for every set of operating conditions. In the next step, time series of p and A were phase-averaged across all recorded pin passages (curves in Fig. 7), with corresponding standard deviation shown in form of vertical bars.

Phase-averaged diagrams presented in Fig. 7 indicate significant variability in the mean hydrophone-measured pressure value as rotor pins pass through the observation area. Under all operating conditions, the highest mean value of p was observed within the time interval 1.2 ms $< t <$ 1.8 ms. Since the passage of rotor pins past the hydrophone always occurred at $t = 1.0$ ms, the rising mean pressure around this time can be explained by a pressure surge induced by approaching pins, while further increases in pressure (and standard deviation thereof) after the pin passage can be attributed to the collapse of cavitation structures – note a reduction in the value of A. In most presented cases, a somewhat inverse relation between pressure p and cavitation cloud area A can be observed, as A mostly increases when p decreases and vice versa. This suggests an interdependence of measured pressure and cavitation area, meaning that cavitation in the wake of moving pins is likely to affect hydrophone pressure readings significantly or even predominantly. On the other hand, pressure pulsations induced by sources other than cavitation (e.g., due to unsteady gap flow when rotor pins pass across stator pins) may also affect the collapse dynamics of cavitation structures.

The effect of individual operating parameters on HC characteristics can be analyzed with respect to diagrams shown in Fig. 7 and integral parameters presented in Table 2. Evidently, the arithmetic mean of the phase-averaged profile of pressure standard deviation (S_p, Table 2) is relatively constant regardless of operating parameters, suggesting similar amplitudes of pressure fluctuations. On the other hand, the mean of the phase-averaged profile of cavitation cloud area standard deviation (S_A) can be seen to increase with pin rotational speed and surface

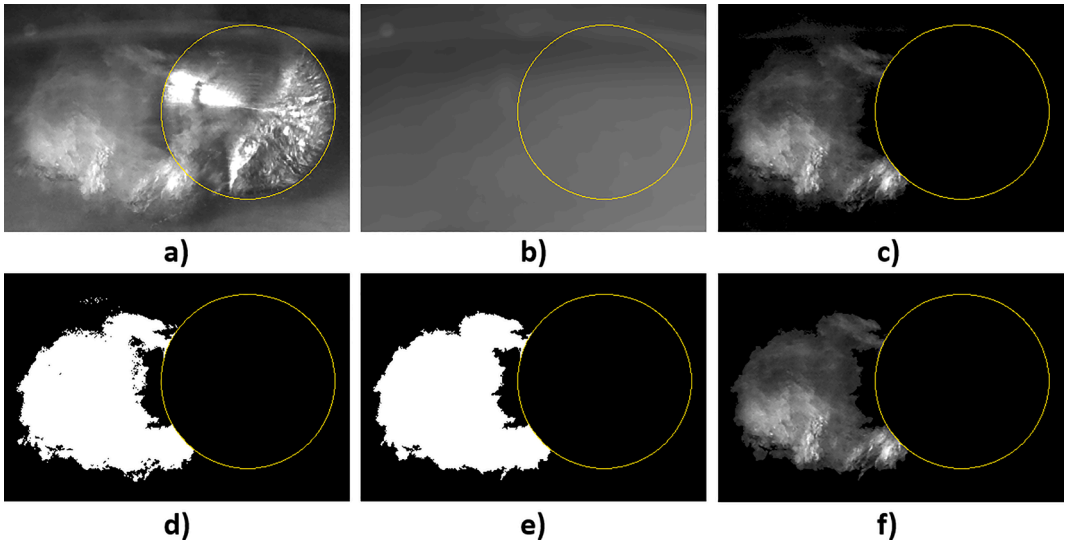

Fig. 5. Image processing steps to determine the extent of vapor clouds attached to the rotor cylinder (position marked by a circle): a) raw image, b) mean background image, c) difference (image (a) - image (b)), cylinder area replaced by a circular mask, d) thresholding to create a mask of vapor cloud extend (white), e) morphological closing, f) difference image intersected with image (e) to verify the correctness of vapor segmentation.

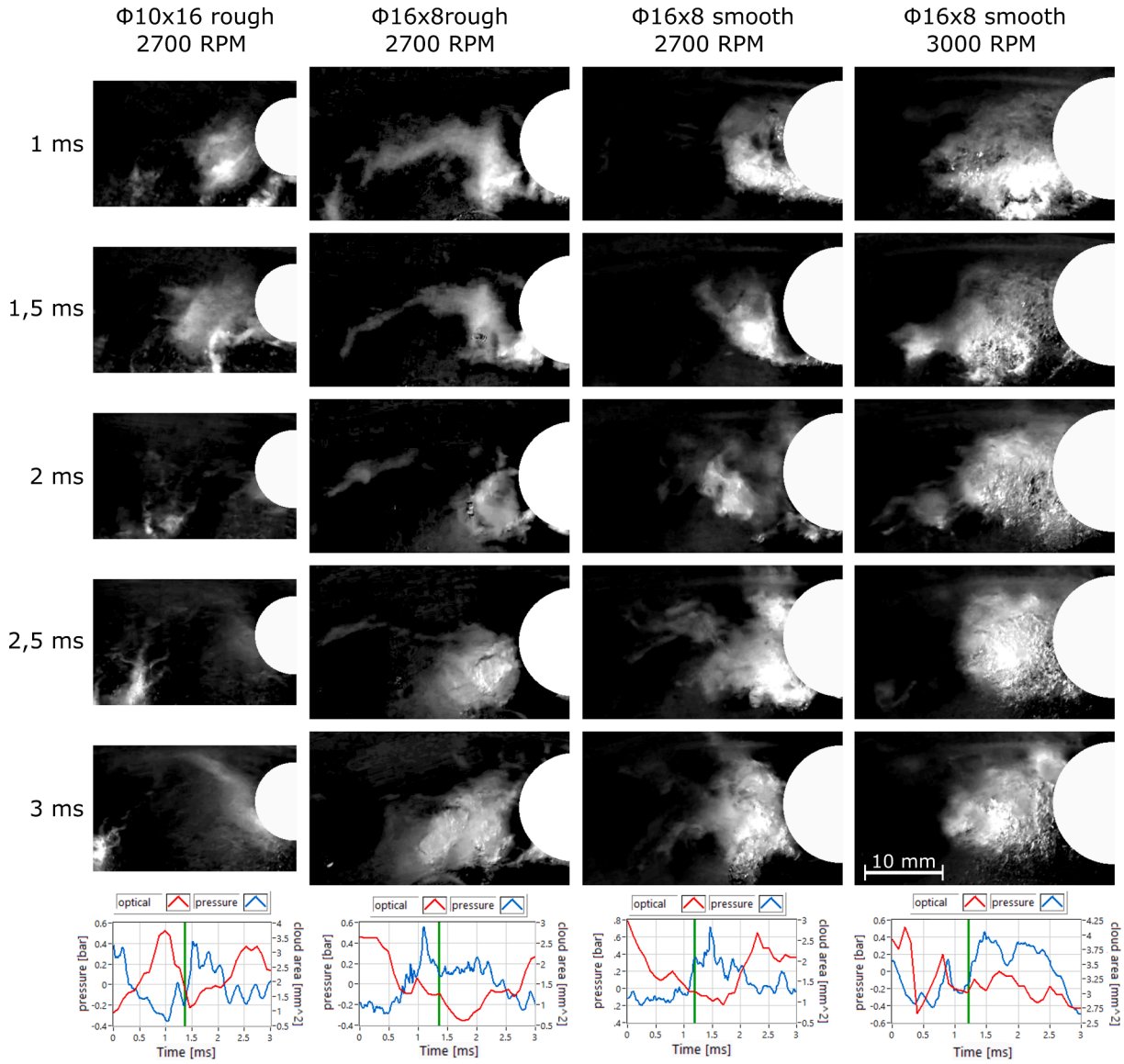

Fig. 6. Cavitating flow behind rotor pins for various RGHC layouts and operating conditions at selected times *t*. Cavitation number: $\sigma = 0.32$ (2700 RPM measurements); $\sigma = 0.26$ (3000 RPM measurement).

Table 2
Characteristic cavitation parameters from time series analysis.

Rotor pin layout	n (RPM)	S_p (bar)	S_A (mm2)	$\overline{A}$(mm^2)	p_{max} - p_{min} (bar)	A_{max} - A_{min} (mm2)
Φ10 mm × 16, rough	2700	0.144	0.550	1.388	0.151	0.553
Φ16 mm × 8, rough	2700	0.125	0.576	1.528	0.397	0.806
Φ16 mm × 8, smooth	2700	0.130	0.474	1.883	0.525	0.741
Φ16 mm × 8, smooth	3000	0.128	0.665	3.657	0.663	0.787

roughness, indicating an increase in either rate or intensity of cavitation structure collapse. Another important metric is the difference between maximum and minimum phase-averaged values of p and A (p_{max}-p_{min} and A_{max}-A_{min}, respectively - Table 2). A high difference value implies a more unsteady cavitation process with higher amplitudes of pressure and cavitation area fluctuations. This and a relatively low mean cavitation area ($\overline{A}$) suggests that the measurement with 16 rotor pins of 10 mm diameter has produced cavitation of lesser intensity than measurements with 8 rotor pins of 16 mm diameter.

Among the 16 mm pin measurements, the rotational speed appears to have a significant effect on cavitation intensity as the values of p_{max}-p_{min}, A_{max}-A_{min} and $\overline{A}$ all increase when the speed is raised from 2700 RPM to 3000 RPM. These findings confirm our visual observations with respect to Fig. 6. As for the effect of pin surface roughness, the rough surface measurement is characterized by higher A_{max}-A_{min}, but lower p_{max}-p_{min} and $\overline{A}$ as opposed to the smooth surface measurement. Although the surface roughness does not appear to significantly enhance the cavitation aggressiveness in our experiments, its effect should be further investigated in future studies. It is well known that the drag coefficient of a rough-surfaced cylinder can decrease substantially due to the onset of drag crisis in high Reynolds number flows [33], potentially reducing the energy consumption for propulsion of the pinned disc.

Besides one-dimensional phase averaging of G and σ, additional characterization of the cavitating flow mechanism is possible by analysis of two-dimensional G and σ scalar fields. For this purpose, the normalized mean and standard deviation of difference images gray level as

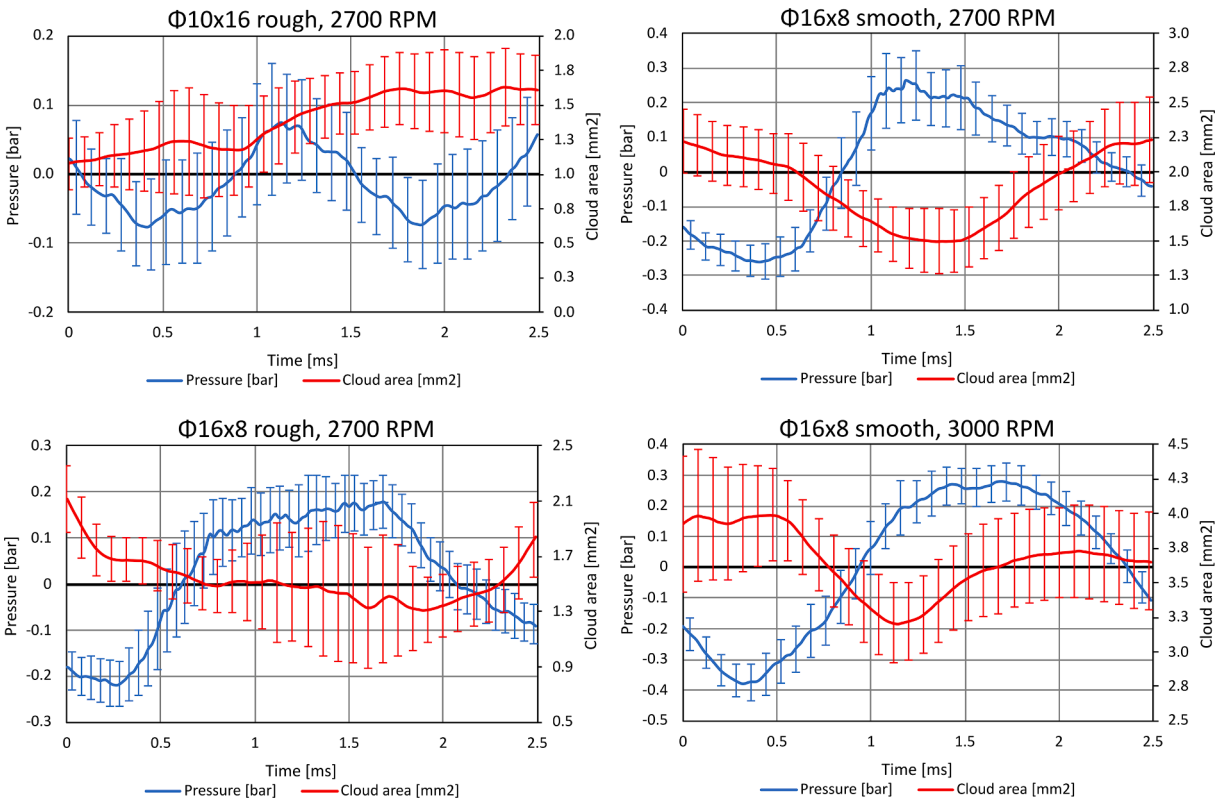

Fig. 7. Phase-averaged time series (profiles) of hydrophone pressure and cavitation cloud area. Rotor pins pass hydrophone position at t = 1.0 ms.

presented in Fig. 5c (represented by G_{pn} and σ_{pn}, respectively) will be calculated by phase averaging at two different rotor pin positions $0 \leq \psi < 1$ relative to the stator pins. Positions directly above a stator pin and halfway between two stator pins correspond to $\psi = 0$ and $\psi = 0.5$, respectively. G_{pn} and σ_{pn} were calculated by Eqs. (1) and (2), respectively.

$$G_{pn}(x,y,\psi) = \frac{1}{G_{max}} \frac{1}{M} \sum_{m=1}^{M} G(x,y,\psi) \tag{1}$$

$$\sigma_{pn}(x,y,\psi) = \frac{1}{\sigma_{max}} \sqrt{\frac{1}{M} \sum_{m=1}^{M} \left(G(x,y,\psi) - \overline{G}(x,y,\psi) \right)^2} \tag{2}$$

In Eqs. (1) and (2), normalization is carried out with respect to the maximum mean and standard deviation of the image gray level (G_{max} and σ_{max}, respectively). Phase averaging is performed across M images where a rotor pin is at a certain position ψ (for rotors with 8 and 16 pins, M ≈ 200 and M ≈ 400, respectively). G_{pn} calculated by Eq. (1) will be assumed proportional to the normalized vapor concentration, while the standard deviation thereof (σ_{pn}) will be a measure of cavitation and turbulent intensity. Note that a high local value of σ_{pn} can occur either due to rapid collapses and rebounds of cavitation structures, or due to strong advection of these structures.

In Fig. 8, the scalar fields of G_{pn} and σ_{pn} are shown for the four RGHC operating points and the two ψ positions. Evidently, at a given rotational speed, rotor pins with larger diameter (namely, 16 mm) produce cavitation clouds with higher mean vapor concentration and higher standard deviation thereof, implying a larger extent and intensity of cavitation. This finding consistent with analysis of integral cavitation parameters presented regarding Table 2. However, the RGHC rotor in operating point with $D_R = 10$ mm shown in Fig. 8 comprised 16 pins while there were only 8 rotor pins in operating points with $D_R = 16$ mm, suggesting twice as many cavitation clouds for the former. Consequently, further investigation is needed to draw conclusions regarding the optimal pin diameter.

Comparing the operating points with $D_R = 16$ mm, results presented in Fig. 8 suggest a significant increase in both G_{pn} and σ_{pn} as well as the length and area of attached cavitation cloud when rotational speed is increased from 2700 RPM to 3000 RPM. This is expected as an increase in the rotor rotational and circumferential speed causes the cavitation number (σ) to drop, leading to a more intense cavitation. However, the ($D_R = 16$ mm, n = 3000 RPM) operating point was not subsequently investigated for chemical effects of WW disintegration because the instantaneous power consumption significantly exceeded the power rating of the electric motor.

Finally, the roughness of the rotor pin surface also appears to affect the cavitation process (note a difference in scalar fields compared to smooth pin measurement), although to a lesser extent than pin diameter and circumferential velocity. In operating points with $D_R = 16$ mm and n = 2700 RPM, rough surface pins (second row in Fig. 8) generate more locally concentrated cavitation bubble collapses, while in the case of smooth pins (third row in Fig. 8), the values of G_{pn} and σ_{pn} are more uniformly distributed. The mean cavitation cloud area was slightly higher for smooth surfaced pins, though (Table 2).

Besides the RGHC operating parameters, relative positioning of rotor and stator pins can also be observed to affect the distribution of G_{pn} and σ_{pn}. In all operating points presented in Fig. 8, the area of maximum vapor concentration and standard deviation thereof is slightly inclined towards the adjacent stator pin as the rotor pin undergoes rotation from $\psi = 0$ to $\psi = 0.5$. This is most likely due to the pressure reduction that occurs in the gap region between the rotor pin and the stator pin moving apart from each other as ψ approaches 0.5. This periodically reoccurring low pression zone results in a force acting upon the attached cavitation cloud in a direction roughly transversal to rotor pin movement, thus playing a major role in the mechanism of cloud detachment from rotor pins. In a free flow, the vortex shedding from rotor pins would be expected to occur with the Karman vortex street frequency ($f_v \approx 0.2D/v$ [34]), corresponding to the approximate range of 300–500 Hz for

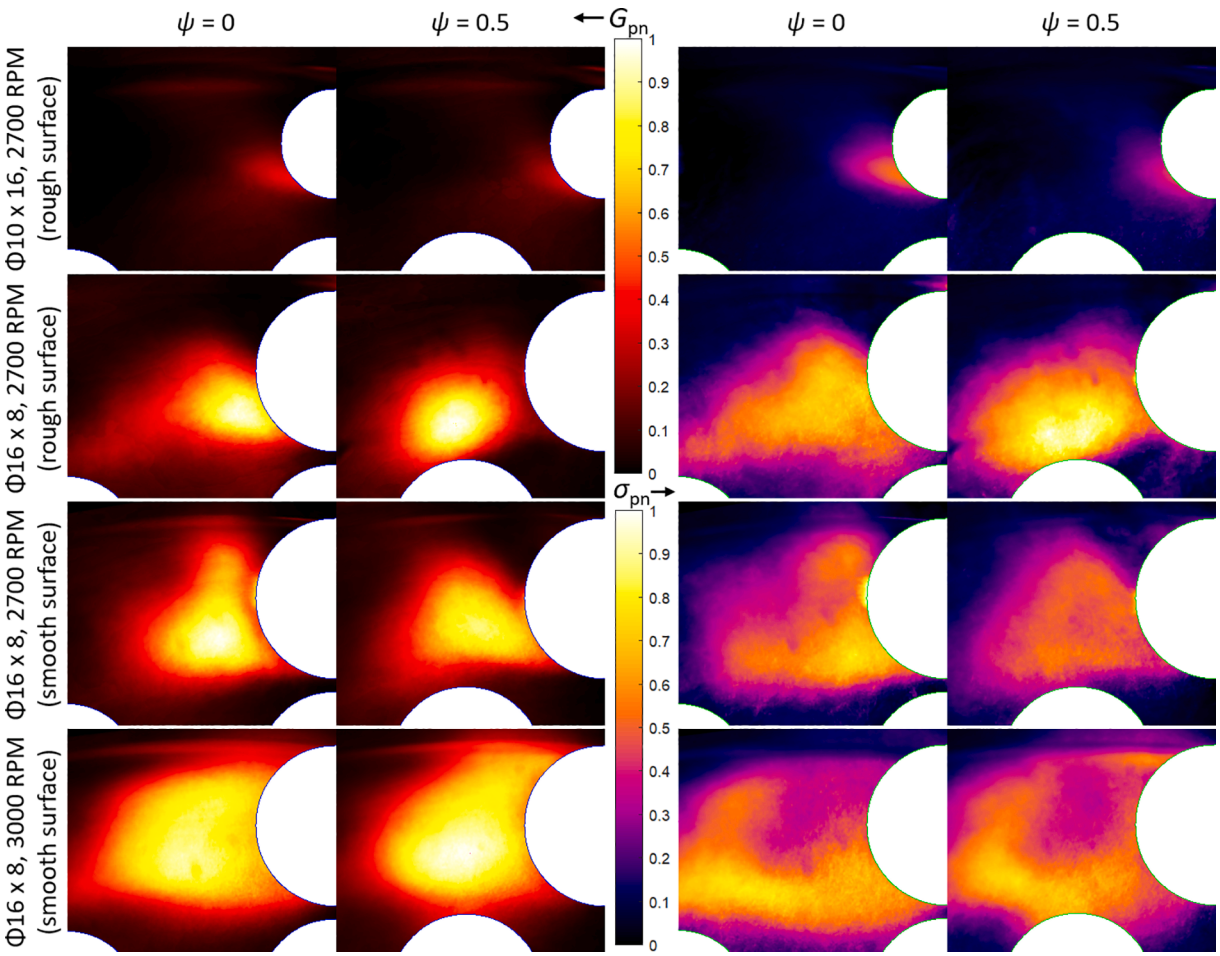

Fig. 8. Phase-averaged mean and standard deviation of relative vapor concentration in four different operating points of the RGHC and at the two rotor pin positions relative to stator pins ($D_S = 12$ mm). Rotor pin diameter: $D_R = 10$ mm in the upper row (68.3 mm arc distance between pin centers) separation, $D_R = 16$ mm in bottom three rows (136.6 mm arc distance between pin centers).

operating parameters used in our experiments. Nevertheless, the actual vortex shedding was observed to occur at a significantly higher frequency equal to the frequency of rotor and stator pins crossing each other (namely, 675 Hz at 2700 RPM and 750 Hz at 3000 RPM), since one shedding event was observed to occur for each stator pin passage by the rotor pin. Therefore, stator pins are a crucial design element of our RGHC despite not directly generating the hydrodynamic cavitation.

Based on the analysis of the HC process in this section, operating parameters for subsequent studies of the COD removal from WW influent were selected as presented in Table 1. Due to the constraint on the number of WW treatment experiments that could be performed, a full variation of operating parameters (rotor speed, pin diameter and surface roughness) was not possible. Instead, three different operating setups were selected (Table 1): 8 rough 16 mm rotor pins at 2700 RPM, 8 smooth 10 mm pins at 3000 RPM and 16 smooth 10 mm pins at 3000 RPM. The first two setups differ in rotor speed, pin diameter and surface roughness, but are very similar in power consumption. On the other hand, the second and the third setup differ only in the number of pins that has nonetheless been shown to significantly affect both integral and cavitation hydrodynamic characteristics.

4.2. Evaluation of WWT parameters and energy efficiency

This section aims to evaluate the chemical and energy efficiency of the HC cavitation process employed in the present study. Depending on the properties of the sample's components, cavitation pattern and intensity, destruction of organic compounds in the liquid can occur via two pathways: (i) free radical attack that can take place inside the cavitation bubble, on the interface between the bubble and the surrounding area and in the bulk solution or (ii) pyrolysis inside or near the bubble [35]. In our experiments, the evaluation of chemical efficiency of various RGHC operating conditions was performed by analysing COD before and after cavitation. Samples were acquired after 15 and 30 cavitation passes (N_p) but since there was no significant difference in COD removal observed at longer N_p, only results after $N_p = 15$ are provided (Table 3). Lack of increased COD removal after $N_p = 15$ suggests that only compounds more resistant to degradation or compounds with hydrophilic physico-chemical properties are left in the WW sample. While a very high number of liquid passes would likely lead to partial removal of these compounds, this is not feasible from the perspective of cavitation time and energy consumption.

Results presented in Table 3 show that in experiments E1-E3 the degree of COD removal ranged from 17 % to 31 %, while sample pH, and conductivity did not change significantly during the experiments. Due to the mixing of the liquid and suspended air bubbles in the cavitation

Table 3
COD and other parameters of untreated and treated WW influent samples.

Experiment	N_p	COD (mg/L)	CR (%)	pH	EC (μs/cm)	DO (mg/L)	T (°C)
0	0	1432	–	7.3	1638	5.7	14
E1	15	1030	28	7.6	1435	10.2	16
E2		990	31	8.1	1888	10.8	16
E3		1186	17	8	1986	10.2	18

chamber, DO concentration increased by about 100 % in all experiments, while the sample temperature rose by only 2 – 4 °C. Since COD represents the amount of both organic and inorganic compounds that can be oxidized in the WW sample, its reduction confirms the oxidation capabilities of these three chosen cavitation regimes. COD removal (CR, Eq. (3)), defined as difference between initial (COD_i) and final COD (COD_{i+t}) normalised to COD_i, suggests that the cavitation set-up of experiment E2 has the strongest oxidation potential (31 % COD removal), although the set-up E1 was only slightly less effective at 28 % COD removal. On the other hand, the set-up E3 only achieved 17 % COD removal despite the higher liquid throughput and power consumption. Since this set-up had 16 rotor pins as opposed to 8 rotor pins of the set-up E2, the only possible explanation for the lower degree of COD removal is a much less aggressive cavitation when the circumferential spacing between pins is reduced. The wake behind cylindrical rotor pins may adversely affect the flow conditions on the downstream pins if the pins are too densely arranged, thus inhibiting the cavitation (note a low cavitation cloud extent and collapse intensity for the setup with 16 × 10 mm rotor pins in Fig. 8). When the pin spacing is doubled, the wake effect likely becomes negligible and the cavitation becomes much more aggressive, achieving a much higher degree of COD removal despite a 50 % reduction in the number of rotor pins. A detailed study of flow velocity and pressure conditions in the rotor–stator interaction zone would be required to determine the optimal pin spacing and is beyond the scope of this paper.

It is worth noting that the COD_i in the present study is substantially higher (1432 mg/L) than the concentration in our previous two studies: 300 mg/L [27] and 648 mg/L [22]. Although the results of these studies cannot be directly compared due to differences in cavitation setups and conditions, it can be observed that when the COD_i concentration is higher, higher degree of COD reduction can be attained (Table 4). The most plausible explanation for this is that higher COD implies a larger probability of short-lived HC-formed $^{\bullet}OH$ radicals reacting with compounds present in WW sample. Radicals that do not encounter such molecules tend to rapidly recombine with each other forming hydrogen peroxide (H_2O_2). Under intense cavitation, a part of H_2O_2 molecules can disintegrate back to $^{\bullet}OH$ radicals, which is why H_2O_2 is often added as a source of radicals [28]. Nevertheless, radicals formed from H_2O_2 experience the same problem of lower statistical probability of reacting with WW influent compounds when COD is low.

The next important measure in evaluation of our RGHC's WWT performance is the energy efficiency of the process. The following quantitative measures will be introduced for its assessment:

$$\mathrm{CODremovalefficiency}: \mathrm{CR} = \frac{(\mathrm{COD}_i - \mathrm{COD}_{i+t})}{(\mathrm{COD}_i)}[\%] \tag{3}$$

$$\mathrm{CODremovalcapacity}: \mathrm{CM} = \frac{(CR - \mathrm{COD}_i)\bullet \mathrm{V}}{\mathrm{t}}\left[\frac{gCOD}{h}\right] \tag{4}$$

$$\mathrm{Energyconsumptionpervolumeoftreatedinfluent}: \mathrm{ECV} = \frac{\mathrm{P}\bullet \mathrm{t}}{\mathrm{V}}\left[\frac{kWh}{m^3}\right] \tag{5}$$

$$\mathrm{SpecificenergyconsumptionpermassofremovedCOD}: \mathrm{EEM} = \frac{\mathrm{P}\bullet \mathrm{t}}{\mathrm{CR}\bullet \mathrm{COD}_i \bullet}\mathrm{V}\left[\frac{kWh}{kgCOD}\right]$$

Based on quantitative measures defined by Eqs. (3) to (6), determined COD reduction, effectiveness, and energy efficiency of our pinned disc RGHC can now be compared to other hydrodynamic cavitation studies where similarly complex samples were processed on cavitation devices of various designs (Table 4). The specific energy consumption per mass of removed COD of all cavitation set-ups from the present study is significantly lower (8.2–13.6 kWh/kg COD) than in other presented studies, including study [36] reporting EEM of 20.6 kWh/kg and our previous study [22] when a value of EEM = 48.3 kWh/kg COD was calculated for the best set-up. This apparently substantial reduction in EEM is however not as much a consequence of the design improvement of the PD RGHC device as it is due to the already mentioned circumstances of the present study: high COD_i and a low number of passes (only 15 compared to 30/60 in our previous study [22] that nonetheless suffices for CR of up to 31 %. Having said that, the dimpled rotor cavitation described in [36] was able to reduce WW COD to an even larger degree (namely, CR = 49%), but was operating at a much higher initial COD (48000 mg/L), so it is difficult to compare CR directly.

In contrast to rotational cavitators, fixed-geometry devices can be seen to consume significantly more energy for a similar COD reduction target. For instance, WW cavitation in a venturi [11] consumed 73.5 kWh/kg COD (about 9 times as much as our experiments E1 and E2) despite an even higher COD_i (2496 mg/L). Venturi and orifice cavitation devices are known to be constrained by a relatively narrow operating range and poor upwards scalability [6], which is why RGHC devices may be one of the very few cavitator designs suitable for large scale, highly energy efficient AOP – not to mention a much greater robustness as larger solid particles dispersed in the WW samples are milled in the rotor–stator interaction zone [22].

Interestingly, the EEM and CM values are almost identical for set-ups E1 and E2 despite the lower CR of the E1 set-up. On the other hand, the set-up E3 has about 40 % lower COD removal capacity and 65 % higher

Table 4
Comparison of WW treatment effectiveness and energy consumption for various hydrodynamic cavitation setups.

Sample type	HC type	COD_I (mg/L)	pH	CR	V (L)	t (min)	N_p	CM (gCOD/h)	ECV (kWh/m^3)	EEM (kWh/kgCOD)	Ref
RefineryWW effluent	orifice 3 bar	142	6–10	37%	6.8	50	50	0.4	4.2	78.5	[10]
	venturi 5 bar	64	6–10	52%	13.3	50	50	0.5	5.5	166.4	
Kitchen	orifice 4 bar	694	3.0	27%	10	120	75	0.9	10.7	57.1	[9]
WW effluent		694	7.0	9%	10	120	75	0.3	10.7	181.4	
Real industrial	venturi 4 bar	2496	4.0	6%	4	120	141	0.1	11.7	73.5	[11]
effluent		1248	4.0	8%	4	120	141	0.3	11.7	119.1	
Laundry WW	Venturi 4 bar	678	9.0	25%	5	90	84	0.6	30.0	179.1	[37]
Wood finishing WW	dimpled rotor 2200 RPM	38,000	6.2	49%	4	20	195	223.4	383.3	20.6	[36]
Urban WW influent	SD 2290 RPM	316	7.8	20%	800	90	30	33.8	8.6	136.3	[27]
	SD 2700 RPM	344	7.9	13%	800	90	30	23.9	14.1	314.5	
Urban WW influent	PD exp. A1	648	8.2	10%	800	58	30	55.2	6.8	101.4	[22]
	PD exp. A2	648	8.2	18%	800	116	60	48.0	13.5	116.7	
	PD exp. B1	635	7.3	21%	800	47	30	139	6.6	48.3	
	PD exp. B2	635	7.3	27%	800	93	60	88.2	13.0	76.0	
Present study	E1	1432	7.6	28%	200	5.88	15	813	3.28	8.25	–
	E2	1432	8.1	31%	200	6.49	15	815	3.62	8.22	
	E3	1432	8.0	17%	200	5.88	15	493	3.99	13.6	

specific energy consumption than set-ups E1 and E2, probably due to already mentioned low pin spacing associated with less favorable flow conditions for cavitation. Results presented so far suggest that the pin diameter and surface roughness are not as crucial parameters in determining the cavitation and energy efficiency of the RGHC as the rotor circumferential speed and pin spacing. As noted by [22], the specific energy cost of RGHC operation (order of magnitude of 1 USD per m^3 of typical WW influent) is still relatively high compared to conventional biological treatment but the improvement of the cavitation process presented in this study has facilitated a further cost reduction.

As an AOP, our cavitation process would be well suited as a pretreatment step to biological treatment in WWTPs treating urban WW, particularly when lacking primary settlers or when receiving high organic load (namely high COD). As seen in Table 4, pretreatment of WW by set-up E2 would remove 31 % COD in 15 passes while consuming 3.28 kWh per m^3 of influent (energy cost of only $\sim$ 0.5 USD/m^3). By combining the RGHC with the biological treatment, the RGHC would not only reduce the COD and lead to smaller amounts of waste sludge, but also assist in the aeration process (note the increase in DO in our experiments) and contribute to degradation/solubilization of particles, facilitating their uptake by microorganisms during the following biological treatment process. This way, better WWT results could be achieved in shorter time, reducing overall operational costs, and increasing the capacity of WWTPs.

5. Conclusions

In this work, the effect of the design and operating parameters of the RGHC with pin disk on the cavitation intensity and COD removal efficiency was investigated. The WWT performance of the RGHC was evaluated on pilot- scale with respect to hydrodynamic and chemical effects. The experimental results lead to the following conclusions:

1. Rotor pin spacing and circumferential velocity are the most important parameters of RGHC design, followed by pin diameter and surface roughness, which play a less significant role for a given cavitator power input. The mean cavitation cloud area and the pressure pulsations induced by its collapse increase with the pin diameter and the circumferential velocity, but may decrease if the pins are arranged too densely.
2. The pressure fluctuations near the rotor pins are related to both the collapse of the cavitation cloud and sources other than cavitation, such as the rotor and rotor–stator pin interaction. An interdependence between phase-averaged pressure and cavitation cloud area was observed, as regions of high pressure coincide with lower mean cavitation cloud area.
3. The number of cavitation passes is a critical process parameter for determining the specific energy consumption of the RGHC. Exceeding the optimal number of passes unnecessarily increases energy consumption with little effect on COD removal. However, the attainable COD removal efficiency increases with the initial wastewater COD.

6. Authors' contributions

J.G. contributed to the new concept of RGHC, designed, developed, and oversaw the manufacturing of the device. M.Z. performed the experiments, analysis, and interpreted the results of WWT parameters. M. D. contributed to image analysis and interpretation of the results. B.Š. conceived and developed the idea of the novel RGHC, coordinated the hydrodynamic part of experiments and helped interpret the results. M.L. organized the experiments on WWTP. B.B. conducted experimental measurements of the RGHC hydrodynamic and cavitation characteristics, performed analysis and interpretation of the results. All authors were involved in the preparation and writing of the manuscript, have contributed to the interpretations of the results, and have approved the final version.

Declaration of Competing Interest

The authors declare that they have no known competing financial interests or personal relationships that could have appeared to influence the work reported in this paper.

Acknowledgements

The authors would like to acknowledge that this project has been co-financed by the Slovenian Research Agency (Core funding No. P2-0401). The authors would also like to thank Petrol d.d. and Domžale-Kamnik WWTP for their support. Furthermore, the authors would like to thank the University of Ljubljana for its financial support within the UL Innovation Fund (Contract No. 820-1/2020-35) and support of Knowledge transfer office UL with patenting of the cavitation device (Application No.: P50434LU00) presented in this paper.

References

[1] M. Gągol, A. Przyjazny, G. Boczkaj, Wastewater treatment by means of advanced oxidation processes based on cavitation – A review, Chem. Eng. J. 338 (2018) 599–627, https://doi.org/10.1016/J.CEJ.2018.01.049.
[2] X. Sun, J. Liu, L.i. Ji, G. Wang, S. Zhao, J.Y. Yoon, S. Chen, A review on hydrodynamic cavitation disinfection: the current state of knowledge, Sci. Total Environ. 737 (2020) 139606, https://doi.org/10.1016/j.scitotenv.2020.139606.
[3] H. Kim, X. Sun, B. Koo, J.Y. Yoon, Experimental investigation of sludge treatment using a rotor-stator type hydrodynamic cavitation reactor and an ultrasonic bath, Processes 7 (11) (2019) 790, https://doi.org/10.3390/pr7110790.
[4] M. Cai, J. Hu, G. Lian, R. Xiao, Z. Song, M. Jin, C. Dong, Q. Wang, D. Luo, Z. Wei, Synergetic pretreatment of waste activated sludge by hydrodynamic cavitation combined with Fenton reaction for enhanced dewatering, Ultrason. Sonochem. 42 (2018) 609–618, https://doi.org/10.1016/j.ultsonch.2017.11.046.
[5] Y. Benito, S. Arrojo, G. Hauke, P. Vidal, Hydrodynamic Cavitation as a low-cost AOP for wastewater treatment: preliminary results and a new design approach, WIT Trans. Ecol. Environ. 80 (2005) 495–503.
[6] B. Wang, H. Su, B.o. Zhang, Hydrodynamic cavitation as a promising route for wastewater treatment – A review, Chem. Eng. J. 412 (2021) 128685, https://doi.org/10.1016/j.cej.2021.128685.
[7] G. Mancuso, M. Langone, G. Andreottola, A critical review of the current technologies in wastewater treatment plants by using hydrodynamic cavitation process: principles and applications, J. Environ. Heal. Sci. Eng. 18 (1) (2020) 311–333, https://doi.org/10.1007/s40201-020-00444-5.
[8] M. Zupanc, Ž. Pandur, T. Stepišnik Perdih, D. Stopar, M. Petkovšek, M. Dular, Effects of cavitation on different microorganisms: The current understanding of the mechanisms taking place behind the phenomenon. A review and proposals for further research, Ultrason. Sonochem. 57 (2019) 147–165, https://doi.org/10.1016/j.ultsonch.2019.05.009.
[9] A. Mukherjee, A. Mullick, R. Teja, P. Vadthya, A. Roy, S. Moulik, Performance and energetic analysis of hydrodynamic cavitation and potential integration with existing advanced oxidation processes: A case study for real life greywater treatment, Ultrason. Sonochem. 66 (2020) 105116, https://doi.org/10.1016/j.ultsonch.2020.105116.
[10] S.B. Doltade, G.G. Dastane, N.L. Jadhav, A.B. Pandit, D.V. Pinjari, N. Somkuwar, R. Paswan, Hydrodynamic cavitation as an imperative technology for the treatment of petroleum refinery effluent, J. Water Process Eng. 29 (2019) 100768, https://doi.org/10.1016/j.jwpe.2019.02.008.
[11] P. Thanekar, P.R. Gogate, Combined hydrodynamic cavitation based processes as an efficient treatment option for real industrial effluent, Ultrason. Sonochem. 53 (2019) 202–213, https://doi.org/10.1016/j.ultsonch.2019.01.007.
[12] P. Jain, V.M. Bhandari, K. Balapure, J. Jena, V.V. Ranade, D.J. Killedar, Hydrodynamic cavitation using vortex diode: an efficient approach for elimination of pathogenic bacteria from water, J. Environ. Manage. 242 (2019) 210–219, https://doi.org/10.1016/j.jenvman.2019.04.057.
[13] X. Sun, X. Xuan, Y. Song, X. Jia, L.i. Ji, S. Zhao, J. Yong Yoon, S. Chen, J. Liu, G. Wang, Experimental and numerical studies on the cavitation in an advanced rotational hydrodynamic cavitation reactor for water treatment, Ultrason. Sonochem. 70 (2021) 105311, https://doi.org/10.1016/j.ultsonch.2020.105311.
[14] X. Sun, J.J. Park, H.S. Kim, S. jin S. Lee, A.S. Om, J.Y. Yoon, Experimental Investigation of the Thermal and Disinfection Performances of aNovel Hydrodynamic Cavitation Reactor, Ultrason. Sonochem. 49 (2018) 13–23. doi: 10.1016/j.expthermflusci.2018.02.034.
[15] Hyunsoo Kim, Bonchan Koo, Xun Sun, Joon Yong Yoon, Investigation of sludge disintegration using rotor-stator type hydrodynamic cavitation reactor, Sep. Purif. Technol. 240 (2020) 116636, https://doi.org/10.1016/j.seppur.2020.116636.
[16] M. Petkovšek, M. Mlakar, M. Levstek, M. Stražar, B. Širok, M. Dular, A novel rotation generator of hydrodynamic cavitation for waste-activated sludge disintegration, Ultrason. Sonochem. 26 (2015) 408–414, https://doi.org/10.1016/j.ultsonch.2015.01.006.

[17] Jose Vilarroig, Raúl Martínez, Elena Zuriaga-Agustí, Salvador Torró, Manuel Galián, Sergio Chiva, Design and optimization of a semi-industrial cavitation device for a pretreatment of an anaerobic digestion treatment of excess sludge and pig slurry, Water Environ. Res. 92 (12) (2020) 2060–2071, https://doi.org/10.1002/wer.v92.1210.1002/wer.1366.
[18] Blahoslav Maršálek, Štěpán Zezulka, Eliška Maršálková, František Pochylý, Pavel Rudolf, Synergistic effects of trace concentrations of hydrogen peroxide used in a novel hydrodynamic cavitation device allows for selective removal of cyanobacteria, Chem. Eng. J. 382 (2020) 122383, https://doi.org/10.1016/j.cej.2019.122383.
[19] Xun Sun, Xiaoqi Jia, Jingting Liu, Guichao Wang, Shan Zhao, Li Ji, Joon Yong Yoon, Songying Chen, Investigation on the characteristics of an advanced rotational hydrodynamic cavitation reactor for water treatment, Sep. Purif. Technol. 251 (2020) 117252, https://doi.org/10.1016/j.seppur.2020.117252.
[20] L.M. Cerecedo, C. Dopazo, R. Gomez-Lus, Water disinfection by hydrodynamic cavitation in a rotor-stator device, Ultrason. Sonochem. 48 (2018) 71–78, https://doi.org/10.1016/j.ultsonch.2018.05.015.
[21] Monika Zubrowska-Sudol, Aleksandra Dzido, Agnieszka Garlicka, Piotr Krawczyk, Michał Stepień, Katarzyna Umiejewska, Justyna Walczak, Marcin Wołowicz, Katarzyna Sytek-Szmeichel, Innovative hydrodynamic disintegrator adjusted to agricultural substrates pre-treatment aimed at methane production intensification—Cfd modelling and batch tests, Energies 13 (16) (2020) 4256, https://doi.org/10.3390/en13164256.
[22] Jurij Gostiša, Brane Širok, Sabina Kolbl Repinc, Marjetka Levstek, Marjetka Stražar, Benjamin Bizjan, Mojca Zupanc, Performance evaluation of a novel pilot-scale pinned disc rotating generator of hydrodynamic cavitation, Ultrason. Sonochem. 72 (2021) 105431, https://doi.org/10.1016/j.ultsonch.2020.105431.
[23] Ye Min Oo, Gumpon Prateepchaikul, Krit Somnuk, Continuous acid-catalyzed esterification using a 3D printed rotor–stator hydrodynamic cavitation reactor reduces free fatty acid content in mixed crude palm oil, Ultrason. Sonochem. 72 (2021) 105419, https://doi.org/10.1016/j.ultsonch.2020.105419.
[24] P.N. Patil, P.R. Gogate, L. Csoka, A. Dregelyi-Kiss, M. Horvath, Intensification of biogas production using pretreatment based on hydrodynamic cavitation, Ultrason. Sonochem. 30 (2016) 79–86, https://doi.org/10.1016/j.ultsonch.2015.11.009.
[25] Martin Petkovšek, Mojca Zupanc, Matevž Dular, Tina Kosjek, Ester Heath, Boris Kompare, Brane Širok, Rotation generator of hydrodynamic cavitation for water treatment, Sep. Purif. Technol. 118 (2013) 415–423, https://doi.org/10.1016/j.seppur.2013.07.029.
[26] Janez Kosel, Andrej Šinkovec, Matevž Dular, A novel rotation generator of hydrodynamic cavitation for the fibrillation of long conifer fibers in paper production, Ultrason. Sonochem. 59 (2019) 104721, https://doi.org/10.1016/j.ultsonch.2019.104721.
[27] Ana Kovačič, David Škufca, Mojca Zupanc, Jurij Gostiša, Benjamin Bizjan, Nina Krištofelc, Marija Sollner Dolenc, Ester Heath, The removal of bisphenols and other contaminants of emerging concern by hydrodynamic cavitation: From lab-scale to pilot-scale, Sci. Total Environ. 743 (2020) 140724, https://doi.org/10.1016/j.scitotenv.2020.140724.
[28] Mojca Zupanc, Tina Kosjek, Martin Petkovšek, Matevž Dular, Boris Kompare, Brane Širok, Marjeta Stražar, Ester Heath, Shear-induced hydrodynamic cavitation as a tool for pharmaceutical micropollutants removal from urban wastewater, Ultrason. Sonochem. 21 (3) (2014) 1213–1221, https://doi.org/10.1016/j.ultsonch.2013.10.025.
[29] Janez Kosel, Matej Šuštaršič, Martin Petkovšek, Mojca Zupanc, Mija Sežun, Matevž Dular, Application of (super)cavitation for the recycling of process waters in paper producing industry, Ultrason. Sonochem. 64 (2020) 105002, https://doi.org/10.1016/j.ultsonch.2020.105002.
[30] Mija Sežun, Janez Kosel, Mojca Zupanc, Marko Hočevar, Janez Vrtovšek, Martin Petkovšek, Matevž Dular, Cavitation as a potential technology for wastewater management – An example of enhanced nutrient release from secondary pulp and paper mill sludge, Stroj. Vestnik/J. Mech. Eng. 65 (11-12) (2019) 641–649, https://doi.org/10.5545/sv-jme10.5545/sv-jme.2019.6328.
[31] P. Kumar, D. Chatterjee, S. Bakshi, Experimental investigation of cavitating structures in the near wake of a cylinder, Int. J. Multiph. Flow. 89 (2017) 207–217, https://doi.org/10.1016/j.ijmultiphaseflow.2016.09.025.
[32] I. Biluš, G. Bombek, M. Hočevar, B. Širok, T. Cenčič, M. Petkovšek, The experimental analysis of cavitating structure fluctuations and pressure pulsations in the cavitation station, Stroj. Vestnik/J. Mech. Eng. 60 (2014) 147–157, https://doi.org/10.5545/sv-jme.2013.1462.
[33] Arne Kilvik Skeide, Lars Morten Bardal, Luca Oggiano, R. Jason Hearst, The significant impact of ribs and small-scale roughness on cylinder drag crisis, J. Wind Eng. Ind. Aerodyn. 202 (2020) 104192, https://doi.org/10.1016/j.jweia.2020.104192.
[34] U. Fey, M. König, H. Eckelmann, A new strouhal-reynolds-number relationship for the circular cylinder in the range $47<Re<2\times105$, Phys. Fluids 10 (1998) 1547–1549, https://doi.org/10.1063/1.869675.
[35] Parag R Gogate, Aniruddha B Pandit, A review of imperative technologies for wastewater treatment I: Oxidation technologies at ambient conditions, Adv. Environ. Res. 8 (3-4) (2004) 501–551, https://doi.org/10.1016/S1093-0191(03)00032-7.
[36] M. Badve, P. Gogate, A. Pandit, L. Csoka, Hydrodynamic cavitation as a novel approach for wastewater treatment in wood finishing industry, Sep. Purif. Technol. 106 (2013) 15–21, https://doi.org/10.1016/j.seppur.2012.12.029.
[37] Vishal V. Patil, Parag R. Gogate, Akash P. Bhat, Pushpito K. Ghosh, Treatment of laundry wastewater containing residual surfactants using combined approaches based on ozone, catalyst and cavitation, Sep. Purif. Technol. 239 (2020) 116594, https://doi.org/10.1016/j.seppur.2020.116594.